

# Application of Magnetohydrodynamic Energy Generation to Planetary Entry Vehicles

Hisham K. Ali<sup>1</sup> and Robert D. Braun<sup>2</sup>  
*Space Systems Design Laboratory, Georgia Institute of Technology*  
 270 Ferst Drive, Atlanta, GA 30331

Proposed missions such as a Mars sample return mission and a human mission to Mars require landed payload masses in excess of any previous Mars mission. Whether human or robotic, these missions present numerous engineering challenges due to their increased mass and complexity. To overcome these challenges, new technologies must be developed, and existing technologies advanced. Mass reducing technologies are particularly critical in this effort. The proposed work aims to study the suitability of multi-pass entry trajectories for reclaiming of vehicle kinetic energy through magnetohydrodynamic power generation from the high temperature entry plasma. Potential mission and power storage configurations are explored, with results including recommended trajectories, amount of kinetic energy reclaimed, and additional system mass for various energy storage technologies.

## Nomenclature

$A$	=	vehicle characteristic area
$A_c$	=	generator area
$B$	=	magnetic field strength
$C_D$	=	drag coefficient
$L_i$	=	generator interaction length
$m$	=	vehicle mass
$n_e$	=	electron number density
$\bar{r}$	=	radial distance between vehicle and Mars center of mass
$u$	=	vehicle velocity
$\beta$	=	ballistic coefficient
$\mu_{Mars}$	=	Mars gravitational parameter
$\rho$	=	atmospheric density

## I. Introduction and Motivation

**F**UTURE missions to Mars such as a Mars sample return mission and potential human mission will require much higher masses than have ever been landed on Mars. Previous Mars missions have relied primarily on Viking era technology for entry descent and landing.<sup>1</sup> The limit of this technology is being reached, with the Mars Science Laboratory (MSL) landing system in 2012 illustrating the difficulty in high mass Martian landings.

To achieve humanity's goals for Mars exploration, significant technology development is required. Mass reducing technologies are particularly critical in this effort. Not only does a larger mass require more fuel to launch, but it also carries significantly more kinetic energy that must be reduced to near zero if the vehicle is to land safely. Previous Mars missions have shown that the majority of the vehicle's kinetic energy is dissipated during the hypersonic phase, about 92.5% in the case of Mars Pathfinder.<sup>2</sup> During this hypersonic phase of entry, there exists a highly heated, ionized flow around the vehicle. The free electrons in the flow can be potentially harnessed to create a sustained, usable electric current via magnetohydrodynamic (MHD) power generation, reclaiming some of the vehicle's dissipated kinetic energy.

<sup>1</sup> Graduate Research Assistant, Aerospace Engineering, AIAA Student Member

<sup>2</sup> David and Andrew Lewis Professor of Space Technology, Aerospace Engineering, AIAA Fellow

MHD vehicle interaction for high speed aerospace applications has been studied since the dawn of the space race, with early theoretical studies dating back to the fifties and early sixties.<sup>3</sup> These studies focused primarily on the flow control applications possible with MHD interaction for purposes such as drag and peak heating modulation. At the time, such studies were limited by available technologies, as the magnetic coils needed to produce the necessary magnetic field were mass prohibitive. Since that time, however, dramatic advances in energy storage and magnetic field generation have been made, and in conjunction with a pressing need to reduce interplanetary launch masses, warrants additional investigation of the topic.

Previous research by Dr. Robert Moses at NASA's Langley Research Center indicates that MHD power generation can be a useful part of future Mars missions.<sup>4</sup> MHD power generation is supported by physics, and numerous power generation schemes have been proposed and studied.<sup>5</sup> Preliminary analysis based on the Mars Pathfinder mission entry trajectory suggests that 100MJ per square meter of electrode area could be generated.<sup>6</sup> However, strong magnetic fields on the order of 1T are required, as well as power equipment to store and handle the generated energy.

The proposed system consists of the following elements: modular MHD generator matrix, electrical current distribution unit, active thermal shield cooling and entry black out mitigation, autonomously powered subsystem for active cooling of temperature sensitive components, resistive load network for heat distribution, oxygen harvesting and separation unit, and rigid, thermo-resistant inflatable containers for oxygen or carbon dioxide storage.<sup>7</sup> Together, these elements create the capability to simultaneously reduce heat shield thermal protection system requirements, reduce entry signal blackout, and generate oxygen for later use on the surface.

For a conventional internal MHD generator, the generated power is linear with ambient electron number density and quadratic with flow velocity.<sup>4</sup> Thus, for a given MHD generator configuration, increased velocity and electron number density will increase output power. The electron number density is primarily fed through aerodynamic heating of the atmosphere, and for a traditional direct entry trajectory is significant for a relatively short period time. For example, the aforementioned 92.5% of kinetic energy lost during the hypersonic phase occurs in less than 60s, presenting difficulties in implementing an energy storage system. It is estimated that for a Mars Pathfinder type space craft, about 14MJ of energy per m<sup>2</sup> of electrode area can be reclaimed during this period; however, this energy generation occurs over about 30s at a high rate of nearly 1 MW.<sup>4</sup> If the energy storage device cannot accept power at this rate, then much of the energy will go to waste. Unfortunately, the ability of an energy storage device to accept energy at a high rate is coupled to its mass, making the direct entry trajectory unattractive for this case.<sup>8</sup>

One proposed alternative is to employ a multi-pass aerobraking entry trajectory to increase the time spent in the atmosphere and harvest energy at a more manageable rate.<sup>4</sup> The challenge of this approach lies in maintaining enough velocity to cause the atmosphere to ionize in order to raise the electron number density to suitable levels. It was found that seeding the flow with small amounts of alkali metals such as potassium or cesium dramatically increases electron number density at concentrations as low as 1%.<sup>5</sup> Seeding the flow while employing multi-pass trajectories would allow for sustained power generation for multiple orders of magnitude more time.

The concept of aerobraking for interplanetary missions has been studied for quite some time, with most initial focus on Mars and Venus.<sup>9</sup> Aerobraking has primarily been utilized for science payloads to assist in transferring the satellite from its hyperbolic interplanetary trajectory to its intended orbit around the target body. Notable missions to Mars that have employed aerobraking include the 1997 Mars Global Surveyor<sup>10</sup>, 2001 Mars Odyssey<sup>11</sup>, and 2006 Mars Reconnaissance Orbiter<sup>12</sup>. These aerobraking maneuvers lasted for significant amounts of time, with the maneuvers taking four months, three months, and five months respectively.

Aerobraking operations that have been studied for MHD power generation take place during significantly shorter periods of time on the order of hours. Previous work by Moses generated multi-pass entry, descent, and landing trajectories, termed E<sup>i</sup>DL, where *i* represents the number of atmospheric passes. These orbit cases were generated by assuming an entry velocity and vehicle mass and varying the system drag area.<sup>4</sup>

In the above case, varying the drag area produced 3, 7, and 11 pass entry paths spending 1881s, 4390s, and 7400s in the atmosphere respectively. The analysis was carried out for a 1000kg Mars Pathfinder class entry vehicle, and yielded an average of 500MJ per pass with a much lower energy generation rate. It is also claimed that future carbon

nanotube based superconducting energy storage devices could store this energy with approximately 200 kg of added system mass, but without this technology, the additional mass requirement would become approximately 3000kg.<sup>4</sup>

It would be of great benefit to extend this analysis to various types of entrance vehicles, and also to attempt to control the number of atmospheric passes through only the initial position and velocity states at the Mars atmospheric boundary. In addition, energy advances in energy storage technologies since the publication of previous results warrants additional review. The contributions contained herein are an effort to achieve these goals. Specifically a model for total energy retained as a function of energy generation rate and amount, a dynamical model that would allow for simulation of multi-pass trajectories and seeded electron number densities, and finally, determination of total converted kinetic energy and additional system mass for various orbit cases, vehicle types, and energy storage technologies.

## II. Relevant Background and Theoretical Approach

### A. Determining the Power Available for MHD Energy Generation

The total energy available via MHD energy generation is the integration of the power available for a MHD generator along a given trajectory. To actually calculate this power generation profile, it is necessary to identify the relevant physical interactions occurring along a given trajectory. These interactions are the gravitational interaction between planetary body and spacecraft, the aerodynamic interaction between planetary atmosphere and spacecraft, and the thermochemical interaction within the atmosphere as the spacecraft moves at supersonic speed. The superimposed effects of these three physical interactions will eventually allow for the definition of the position state, velocity state, and electron number density. These states define the total power that can be generated by MHD energy conversion. For a conventional internal MHD generator, the generated power behaves the following scaling law<sup>4</sup>

$$P \propto n_e u^2 B^2 A_c L_i \quad (1)$$

Where  $P$  is the generator power output,  $n_e$  is the ambient electron number density,  $u$  is the flow velocity,  $B$  is the magnetic field strength,  $A_c$  is the generator area, and  $L_i$  is the generator length. For the purposes of this analysis, the magnetic field strength will be assumed in all cases to be a constant 0.2 Tesla. The generator area will be assumed to be 1 square meter in all cases as well, with a characteristic length of 1 meter. As a result, the above scaling law can be reduced to a function of electron number density and velocity only.

The remaining tasks are to find the velocity and electron number density along the trajectory. The velocity can be calculated by defining the system dynamics and integrating to obtain position and velocity. Taking into account the gravitational and aerodynamic interaction, the Equation of motion for the system relative to the Martian center of mass can be written as

$$\ddot{\vec{r}} = -\frac{\mu_{Mars}}{(\vec{r} \cdot \vec{r})^{3/2}} \vec{r} - \frac{\rho(\dot{\vec{r}} \cdot \dot{\vec{r}})}{2\beta} \hat{\vec{r}} \quad (2)$$

where  $\rho$  is the atmospheric density, implicitly a function of altitude and calculated from a relevant Mars atmospheric model, and  $\beta$  is the ballistic coefficient of the entry vehicle, defined below as follows:

$$\beta = \frac{m}{C_D A} \quad (3)$$

where  $m$  is the entry vehicle mass,  $C_D$  is the entry vehicle drag coefficient, and  $A$  is the entry vehicle characteristic area. Since altitude is a function of position and  $\beta$  is constant for a given entry vehicle, Equation 2 is now a system of differential Equations as functions of position and velocity. These Equations can be numerically integrated using a tool such as MATLAB's ode45 to give the position and velocity states as a function of time.

To calculate the electron number density, the atmospheric composition after passing through a shock wave must be calculated. Since the ambient density, pressure, and temperature can be calculated as functions of altitude, and Martian atmospheric species composition is known and assumed to be constant, the addition of velocity fully

specifies the post shock state. A chemical equilibrium solver, in this case NASA's Chemical Equilibrium and Applications (CEA) code, is then used to calculate the post shock state.<sup>13</sup>

Martian atmospheric constituents in order of relative abundance are CO<sub>2</sub> at 95.9%, Ar at 2.0%, N<sub>2</sub> at 1.9%, O<sub>2</sub> at 0.14%, and CO at 0.06%.<sup>14</sup> Post shock species include: Ar, C, N, O, C<sub>2</sub>, N<sub>2</sub>, O<sub>2</sub>, CN, CO, NO, CO<sub>2</sub>, NCO, Ar<sup>+</sup>, C<sup>+</sup>, C<sub>2</sub><sup>+</sup>, N<sup>+</sup>, N<sub>2</sub><sup>+</sup>, O<sup>+</sup>, O<sub>2</sub><sup>+</sup>, CN<sup>+</sup>, CO<sup>+</sup>, NO<sup>+</sup>, and e<sup>-</sup>. Since an equilibrium solver is being used, the particular chemical reaction mechanism by which these processes occur are not needed. Only the initial species, final species, initial atmospheric properties, and velocity are needed. Using these data in conjunction with the atmospheric properties as a function of altitude, the post shock temperature, pressure, and species composition can be calculated as a function of velocity.

Once the species composition, temperature, and pressure are known, the equilibrium electron number density is calculated using the post shock density, molecular weight, and electron mole fraction. Equilibrium electron number density is strongly dependent on the post shock temperature, and the standard Mars atmospheric constituents fail to yield sufficient electron number density for MHD energy generation below velocities of 5 km/s. However, previous work indicates that seeding the flow with a small amount of easily ionizable species such as alkali metals can boost the electron number density. For example seeding the flow in the vicinity of the MHD Generator with 1% potassium by mass results in multiple order of magnitude increases in electron number density.<sup>5</sup> Results for 1% potassium seeded electron number density as a function of vehicle velocity and altitude are presented below as Figure 1

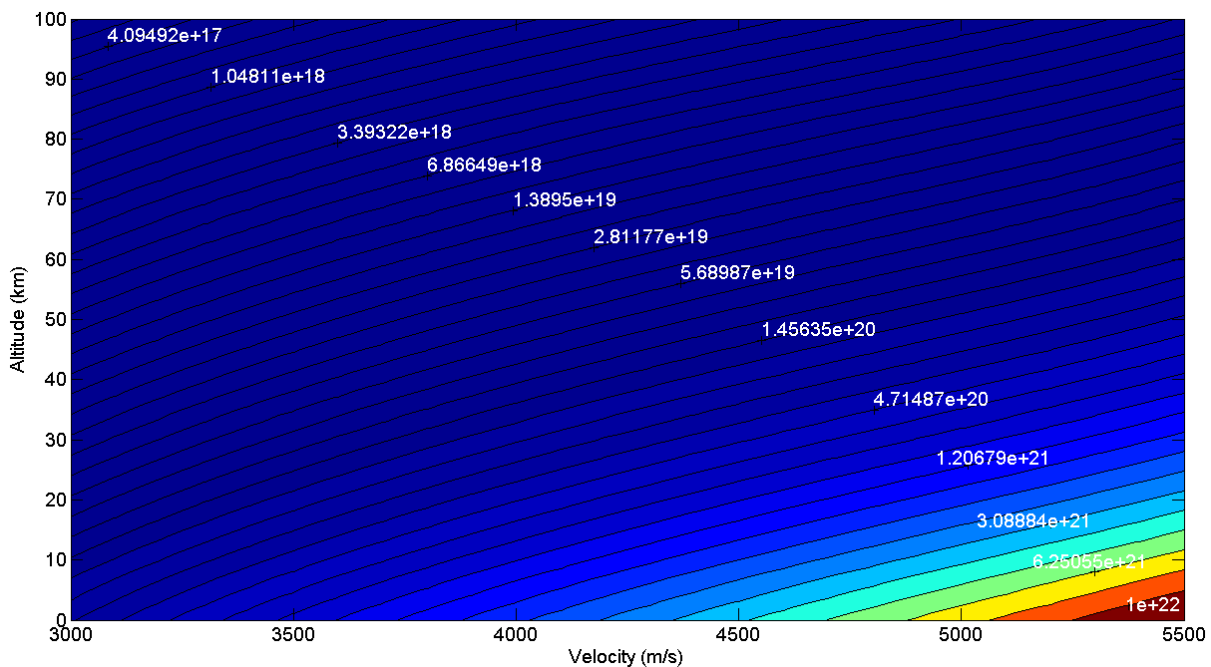


**Figure 1. Seeded electron number density (#/m<sup>3</sup>) as a function of Mars altitude and vehicle velocity.**

After the numerical integration has been done to calculate the trajectory and obtain the velocity and altitude, the electron number density at each point in the trajectory is calculated using the method described above. Then, the power generated can be calculated for each point, giving a power vs. time curve that defines the amount of energy available for that trajectory. This curve is then ready for analysis by the electrical energy storage system model.

## B. Electrical Energy Storage Systems

Electrical energy storage systems are extremely diverse in their mechanisms and applications. These systems can be mechanical, chemical, and electrodynamic in mechanism, while others still are combinations of these elements. Applications for electrical energy storage systems range from mobile devices to large water retention ponds capable of powering entire cities for long periods of time.<sup>16</sup> With such a diversity in mechanisms and applications, appropriate performance objectives upon which to evaluate electrical energy storage systems are challenging to develop. This problem is particularly troublesome for systems under development that may have an ill-defined application profile.

Examples of common electrical energy storage system performance parameters include mass, endurance, power capacity, longevity, and heat generation. For example, while longevity as measured by charge and discharge cycles may be an issue for chemical electrical energy storage systems such as batteries, it may not be an issue for physically based energy storage systems such as pumped hydroelectric storage. However, batteries have a clear advantage in mobility and mass, while pumped hydroelectric storage is suitable for static mass unconstrained situations such as municipal power generation.<sup>16</sup>

Thus, if one is to properly model a given energy storage system's performance, much effort must first be expended to properly define and identify parameters most important to a particular application. The application being presently considered is a flight application, and thus mass is expected to play an extremely important role in the performance of such an energy storage system. In addition, although electrical energy storage system parameters such as longevity and heat generation are important, the assessment of their impact requires detailed system design information that is outside the scope of this analysis and typically not known without precise knowledge of the energy usage loads and flight system geometry. The total amount of electrical energy generated will allow for estimation of the size of energy storage device needed; however, as mentioned earlier the electrical energy generation for this application may occur at a relatively high rate that will place requirements on system power capacity as well.<sup>16</sup>

Thus, for the purposes of this analysis, total energy system mass is determined to be the most important parameter. If some total amount of energy is to be generated at a certain rate, mass and energy requirements can be calculated. Both total energy storage capacity and discharge power capacity for an electrical energy storage system can be related to system mass by defining mass specific versions of each of these properties. Typical units are watt hours per kg and watts per kg for specific energy storage and power discharge capacity. Although electrical energy storage systems for a given type may vary in their values for the aforementioned parameters, there is typically a range for each parameter that is considered appropriate for a given technology. These values are determined experimentally and continually evolve as new developments in energy storage techniques come to fruition. These ranges can be used to define a best, average, and worst case scenario for a given technology.

As mentioned earlier, there are large a number of electrical energy storage systems in use; however, given the present flight application, there are a smaller number of energy storage systems that are appropriate. The electrical energy storage systems categories that will be considered in this analysis are batteries, capacitors, and miscellaneous devices such as flywheels and super conducting magnetic energy storage.

Batteries are used in a variety of both static and mobile situations, with applications ranging from low to high power. They involve some sort of chemical reaction, that when activated generates electricity. Although the bulk system performance for a battery is a function of complex multi-step reactions in reality, the performance as measured by power and energy density can be abstracted to a rough function of mass. Batteries under consideration are chosen as being representative, though not exhaustive, of the rechargeable technologies available and listed in order of age include lead acid, nickel cadmium, and lithium ion. Each of these systems has a characteristic performance, proven robustness, and longevity that makes them representative of the category from a performance analysis perspective.

Capacitors are another electrical energy storage system type that has the potential for portability, but unlike batteries, they store their energy in an electrical field generated internally. They can thus be said to have an electrodynamic energy storage mechanism. Capacitors as typically seen in consumer electronics are electrolytic capacitors, consisting of two metal plates a certain distance apart filled with a dielectric material. They can be made to withstand extremely high voltage and energy storage rates, but their specific total energy storage capacity is usually poor. Recently, new types of capacitors that do not involve conventional dielectrics, but instead achieve much higher capacitance through separation of charge along extremely short distances or electrochemical reactions. These capacitors, termed super or ultracapacitors, have energy charge and discharge rates comparable to conventional capacitors, but have much higher specific energy values. The performance ranges for both types are distinct, and together these ranges serve as useful characterizations for the technology.

Other electrical energy storage systems are considered in this analysis. Some of these systems are exotic in nature and are quite new. One example is superconducting magnetic energy storage. In this storage technique, the resistance less property of a superconducting material is used to facilitate an extremely high loop current that results

in a dense magnetic field. This magnetic field stores the electrical energy. Due to their superconductivity, such systems have very high power discharge and charge rates, and acceptable energy storage density. Disadvantages, however, include the cryogenics usually necessary to achieve superconductivity, the effect of the strong magnetic field on neighboring electronics, and overall system weight. Superconducting magnetic energy storage system performance may be enhanced by exploiting superconductivity of carbon nanotubes, reducing system weight while increasing specific energy and power capability.<sup>17</sup> Another type of electrical energy storage system considered is a flywheel based system, where electrical energy is stored mechanically, typically with the assistance of magnetic bearings. Such a system can store a relatively large amount of energy with minimal thermal loss and high discharge rates when needed. This system may also have additional effects on flight vehicles with regards to stability and control owing to the large rotating mass.

In summary, electrical energy storage systems performance can be represented as mass specific energy and discharge power capacity. For the present application of power generation and energy storage, charge power capacity and discharge power capacity are assumed to be roughly equal, simplifying the analysis. One way in which to visualize the performance of these systems is to plot the specific power vs. the specific energy storage capacity. Such a plot is termed a Ragone plot and is very useful for selecting power systems. For the application being considered, good choices generally lie to the top right of the chart, while poorer choices lie to the bottom left. A Ragone plot generated from industry data for the energy storage devices being considered is presented below as Figure 2.

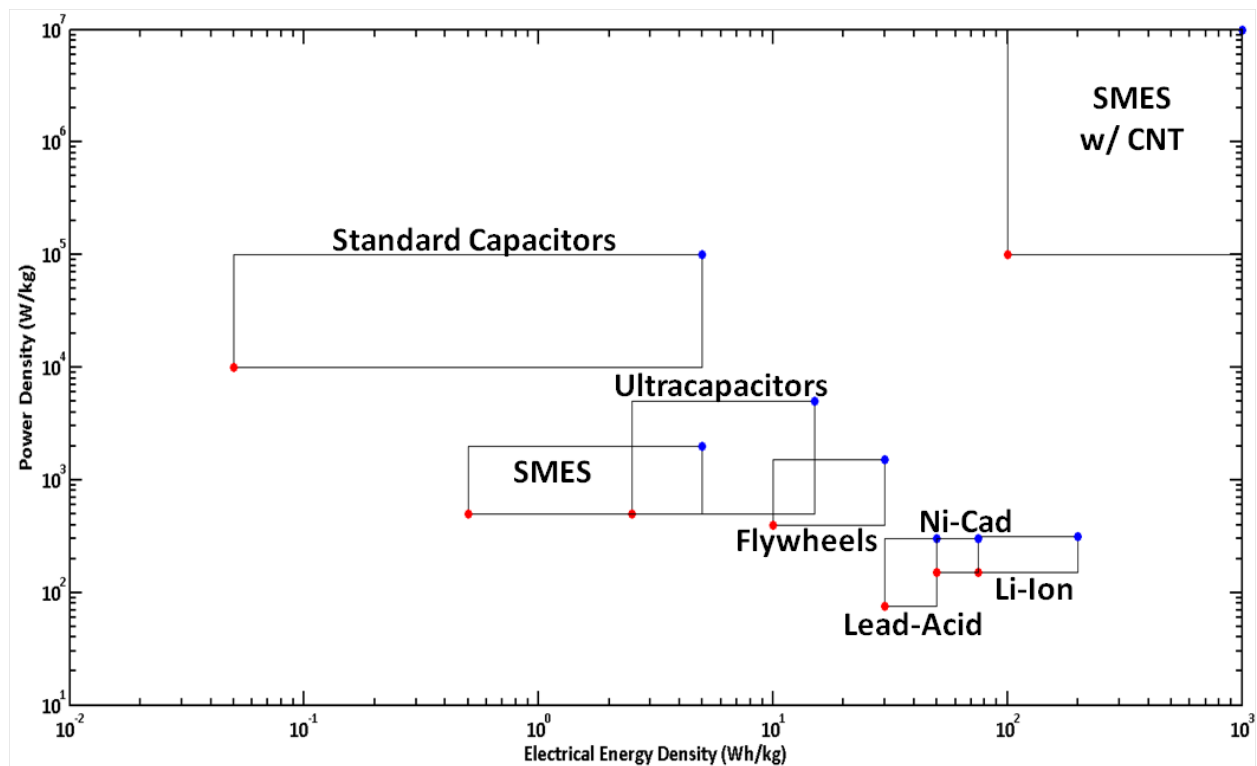


**Figure 2. Ragone plot for electrical energy storage systems under consideration.**

The plot presented above includes highlights of best and worst case scenarios, as represented by the red and blue dots respectively. These values do not necessarily represent any real device in particular, rather only the limits of a particular technology. This plot gives the necessary information to calculate the electrical energy storage system mass for a power vs. time profile.

### III. Methodology and Experimental Design

#### A. Dynamical Model Implementation and Power Profile Construction

The aforementioned approach is implemented numerically in MATLAB. The temperature and pressure are written as simple functions of altitude based on relevant Mars atmospheric data, with temperature following a linear profile and pressure following an exponential one. The Martian atmospheric composition is known to be relatively constant with altitude<sup>14</sup> and in conjunction with the ideal gas law allows for the calculation of the density variation with altitude as well. The specification of the ambient temperature, pressure, composition, density completes all relevant Martian atmospheric inputs into the model.

With the relevant Martian atmospheric conditions specified, the dynamical model described in Equation 2 is implemented in MATLAB using the ode45 integration function. Given initial conditions, the model calculates the position and velocity states as functions of time until the spacecraft's trajectory intersects with the Martian surface. In addition, the model is also set up to record and count each instance in which the spacecraft exits or leaves the Martian atmospheric boundary, taken in this case as an altitude of 100km. This tabulation is important in effectively determining the number of complete orbits made during a multi-pass entry trajectories as well as determining the total time spent in the atmosphere.

**Table 1 Test Vehicle Configurations**

Property	Moses Test Vehicle <sup>4</sup>	Mars Pathfinder	Mars Science Lab
Mass (kg)	1000	582	2800
$C_D$	0.40	0.40	0.67
$A$ (m <sup>2</sup> )	7.00	5.52	16.6
$\beta$ (kg/m <sup>3</sup> )	357	264	252
$V_{\text{entry}}$ (km/s)	5.00	5.00	5.00

The test vehicle configurations considered in this analysis are presented above as Table 1. For each configuration, the initial altitude and velocity was 100 km and 5 km/s respectively, and multi-pass entry trajectories were found experimentally by varying the initial flight path angle and using the aforementioned model to determine the number of passes and the total time in atmosphere. The result was a series of entry trajectories for each configuration, with number of passes ranging from two to ten. The initial conditions for these trajectories are presented below as Table 2.

**Table 2 Initial Conditions for Each Test Vehicle Configuration at 100 km Altitude and 5 km/s Velocity**

Number of Complete Passes	Moses Test Vehicle		Mars Pathfinder		Mars Science Lab	
	$\gamma_{\text{entry}}(^{\circ})$	Time in Atmosphere(s)	$\gamma_{\text{entry}}(^{\circ})$	Time in Atmosphere(s)	$\gamma_{\text{entry}}(^{\circ})$	Time in Atmosphere(s)
2	-5.50	1350	-5.10	1313	-5.00	1321
4	-4.65	2017	-4.20	1900	-4.10	1888
6	-4.05	2549	-3.55	2346	-3.50	2309
8	-3.60	2965	-3.05	2676	-2.95	2626
10	-3.20	3312	-2.70	2961	-2.55	2852

Each initial condition specifies the position and velocity states throughout the corresponding trajectory, giving the altitude and speed at each point. The electron number density is calculated using NASA's CEA code to solve the post shock thermochemistry problem. Inputs are the freestream velocity, atmospheric composition, seed particle amount, and ambient atmospheric pressure and temperature. The atmospheric composition is as noted previously, and the seed particle is left as 1% mass fraction potassium as indicated in previous studies.<sup>4</sup> The ambient pressure and temperature can be generalized as functions of altitude, such that the electron number density is essentially a function of altitude and velocity only. In order to expedite computation for multiple runs, a lookup table for electron number density as a function of altitude and velocity is generated, with altitude varying from 0 to 100 km in 1km increments and velocity varying from 3000 – 5500 m/s in 100 m/s increments. These values cover the range of conditions and velocities suitable to MHD energy generation<sup>4</sup>, with final electron number density linearly interpolated based on the Table values.

## B. Electrical Energy Storage System Performance Model

A model has been created that calculates the electrical energy storage system mass for a given power generation profile and energy storage system type. It does so by integrating the power generation vs. time profile curve to calculate the total energy available for storage while also noting the peak energy generation power. As shown in Figure 2, both power and energy requirements define energy storage system mass. Thus, there are two possibilities, power capacity driven mass, and energy generation driven mass. Both approaches must be taken, and the final stored energy is assessed relative to the initial amount of energy. From the system mass and relative energy conversion metrics, an educated assessment can be made with regards to what energy storage system mass is most advantageous for a given technology. The numerical values for Figure 1 are summarized below as Table 3

**Table 3 Electrical Energy Storage System Performance Data**

EES System	Minimum Wh/kg	Maximum Wh/kg	Minimum W/kg	Maximum W/kg
Lead Acid	30	50	75	300
Nickel Cadmium	50	75	150	300
Lithium Ion	75	200	150	315
Capacitors	0.05	5	10,000	100,000
Ultracapacitors	2.5	15	500	5,000
SMES	0.5	5	500	2,000
SMES w/ CNT	100	1,000	100,000	10,000,000
Flywheels	10	30	400	1,500

The minimum and maximum pairs in Table 3 above define worst and best cases respectively. In addition, an average case can be generated that is exactly between the two. The result is three distinct performance cases for each technology, and is selectable within the model by the user. The end result is to generate values for power and energy density given selections for energy storage system type and performance scenario. These processes are described below as Figure 3.

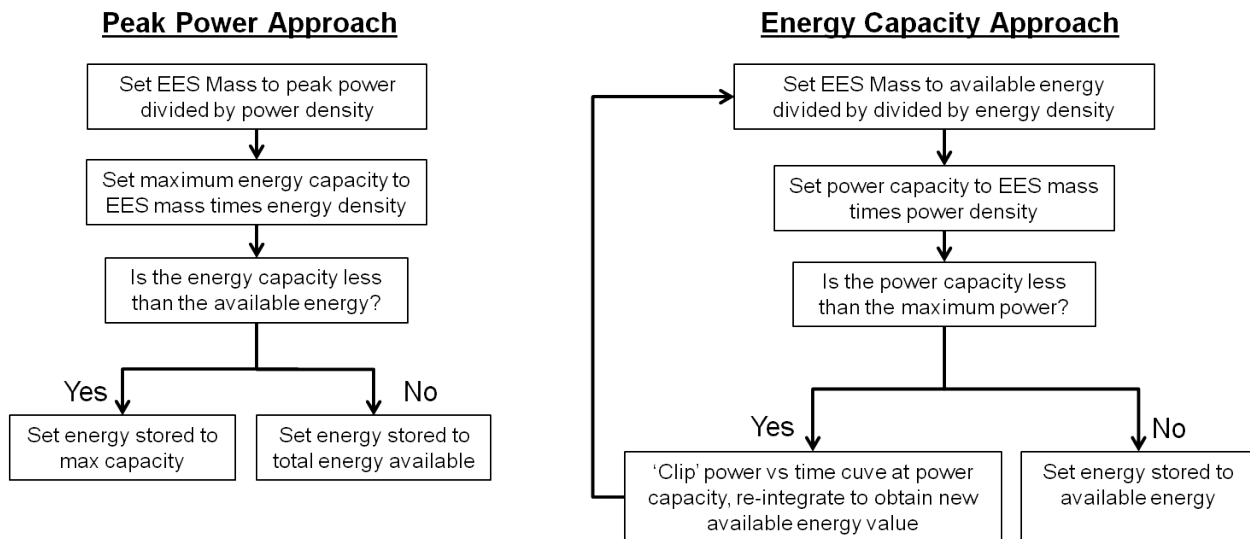


**Figure 3. Electrical energy storage system model flowchart.**

As shown in Figure 3, there are two approaches to finding energy storage system mass. The first approach is simpler and involves defining system power capacity as equal to the maximum energy generation rate from the given power profile. Dividing this system power capacity by the specific power capacity for the technology under consideration results in the system mass. Total stored energy is calculated by multiplying this mass by the specific energy capacity of the technology under consideration, and this value is compared with the total energy available. Depending on the technology, this approach may generate a very high or very low mass and very high or very low percent available energy stored.

The second approach is somewhat more complicated and involves using the total available energy to drive system mass. An initial guess for the system mass is set by dividing total available energy by specific energy capacity for the technology in question. This initial guess for system mass is then used to calculate the power capacity of this system. If the power capacity is above the maximum power for the power profile, no further action is taken, otherwise, the power generation profile must be ‘clipped’ at the maximum power capacity rate for the system. Thus, a new power profile curve and associated total energy is generated, requiring that the initial guess for the mass be modified. This process must be completed iteratively until a converged value for energy storage mass is found. At the completion of the process, the final mass determines the amount of energy stored, and it can be compared with the original amount of energy available from the power generation profile.

At the conclusion of this process, the model outputs the system mass and converted energy using both approaches in addition to the total energy available for conversion. Different technologies may result in one or the other approach being better than the other. For this analysis, the highest percent energy retained is chosen. Finally, there is an option to limit the total energy storage system mass to come predefined value, taken as 10% for this analysis.

A sample power generation profile for the Moses Entry Vehicle direct entry case from previous work by Moses at NASA’s Langley Research Center is presented below as Figure 4.

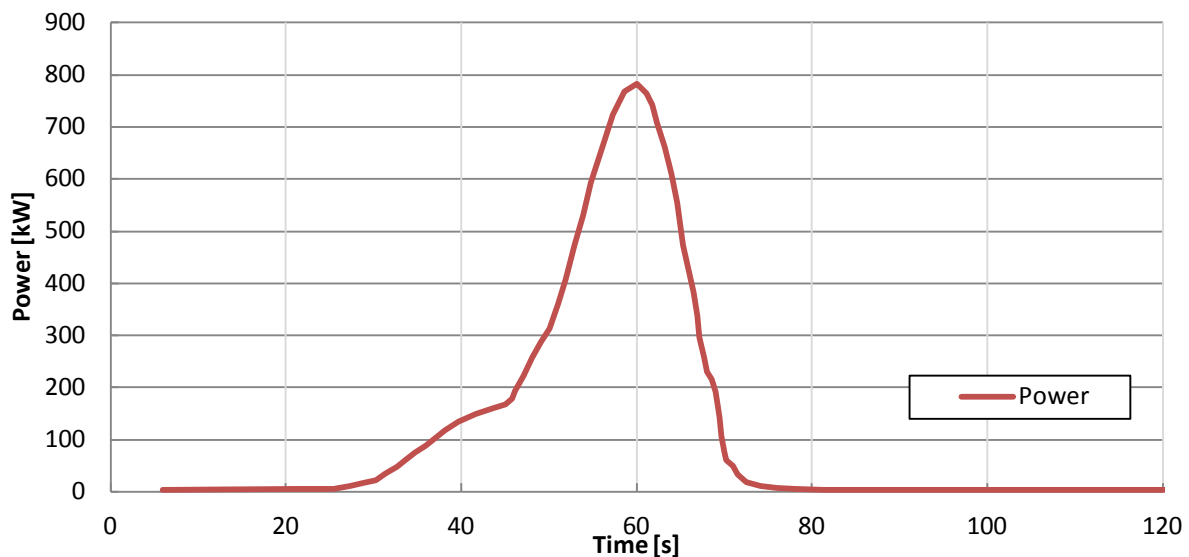


Figure 4. Direct entry power generation profile for Moses test vehicle.<sup>4</sup>

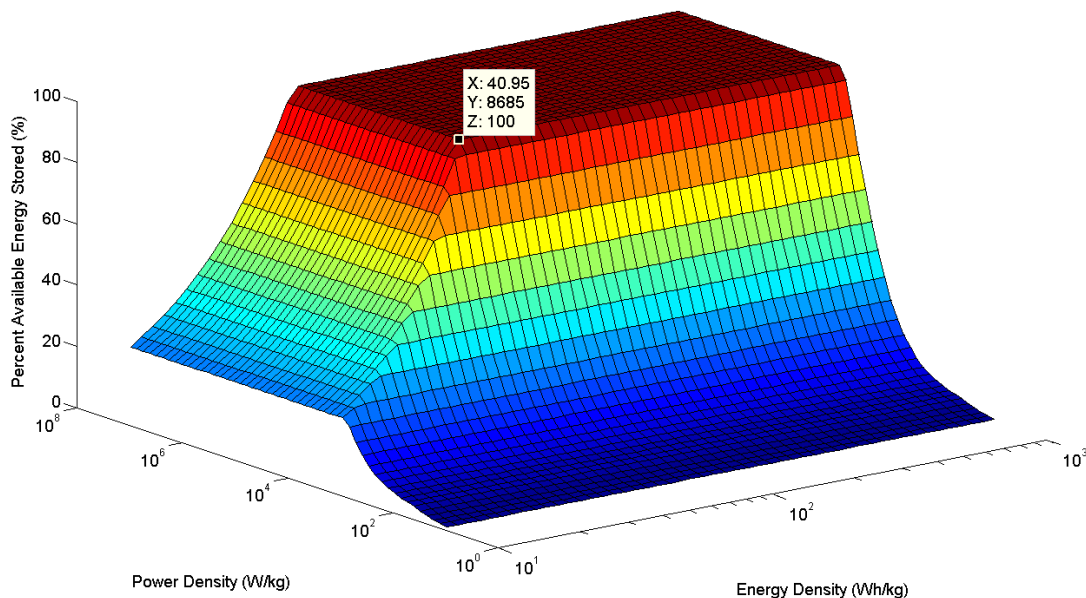
Analysis of the aforementioned power profile assuming no constraints on energy storage mass and average performance for each energy storage technology yields the mass data given in Table 4 below

Table 4 Moses Test Vehicle Direct Entry Electrical Energy Storage System Mass

EES Technology	Mass (kg)	Calculation Method
Li-Ion	3368	Peak Power
Lead Acid	4176	Peak Power
NiCad	3480	Peak Power
Capacitor	1551	Max Energy
Ultracapacitor	447.5	Max Energy
SMES	1424	Max Energy
SMES w/ CNT	7.120	Max Energy
Flywheel	824.2	Peak Power

Many of the energy storage system masses in Table 4 are above the original vehicle mass of 1000kg. In many cases, the mass is very high due to the limited power capacity in comparison to the energy capacity or vice versa. Since the energy storage system mass is a function of only two parameters, power density and energy density, a surface plot of

the total energy stored while limiting mass to 10% of overall vehicle mass can be generated, given as Figure 5 below.



**Figure 5. Percent available energy stored for Moses test vehicle direct entry case, mass constrained to 100kg.**

As can be seen in Figure 5, the energy storage system is incapable of storing the available energy up to a certain point, marked with a data cursor. This point is of interest because it defines the minimum performance characteristics necessary for an energy storage system to satisfy a certain mass constraint and store all of the available energy without wasted storage capacity.

#### IV. Results and Discussion

In the following analysis, results are presented for the three previously described vehicle configurations for a variety of passes. Tabulated values include the generated energy, minimum energy storage system performance required to fit within a 10% of vehicle mass envelope, and selected trajectories and associated unconstrained energy storage system masses for a variety of technologies. Tabulated values are presented below as Tables 5 through 7

**Table 5 Moses Test Vehicle Results**

Passes	Time in Atmosphere (s)	Available Energy (MJ/m <sup>2</sup> )	Energy / Pass (MJ/ m <sup>2</sup> Pass)	Minimum Power Density (W/kg)	Minimum Energy Density (Wh/kg)
2	1355.5	265.3	132.7	8685.1	754.3
4	2026.5	239.1	59.8	4941.7	686.6
6	2566.0	217.7	36.3	3727.6	625.1
8	2977.0	200.3	25.0	2811.8	569.0
10	3334.5	185.9	18.6	2121.0	517.9

**Table 6 Mars Pathfinder Test Vehicle Results**

Passes	Time in Atmosphere (s)	Available Energy (MJ/m <sup>2</sup> )	Energy / Pass (MJ/ m <sup>2</sup> Pass)	Minimum Power Density (W/kg)	Minimum Energy Density (Wh/kg)
2	1315.6	187.1	93.5	11514.0	910.3
4	1903.7	164.6	41.1	6551.3	828.6
6	2352.0	146.3	24.4	4941.7	754.3
8	2684.2	133.1	16.6	3727.6	686.6
10	2951.2	124.0	12.4	2811.8	625.1

**Table 7 Mars Science Laboratory Test Vehicle Results**

<b>Passes</b>	<b>Time in Atmosphere (s)</b>	<b>Available Energy (MJ/m<sup>2</sup>)</b>	<b>Energy / Pass (MJ/ m<sup>2</sup> Pass)</b>	<b>Minimum Power Density (W/kg)</b>	<b>Minimum Energy Density (Wh/kg)</b>
<b>2</b>	<b>1328.9</b>	<b>176.1</b>	<b>88.1</b>	<b>2121.0</b>	<b>184.2</b>
<b>4</b>	<b>1898.5</b>	<b>154.3</b>	<b>38.6</b>	<b>1206.8</b>	<b>167.7</b>
<b>6</b>	<b>2310.5</b>	<b>137.8</b>	<b>23.0</b>	<b>910.3</b>	<b>138.9</b>
<b>8</b>	<b>2645.6</b>	<b>124.5</b>	<b>15.6</b>	<b>686.6</b>	<b>126.5</b>
<b>10</b>	<b>2751.1</b>	<b>115.5</b>	<b>11.6</b>	<b>686.6</b>	<b>115.1</b>

In examining Tables 5 through 7, a few interesting trends can be observed. For all three cases, the amount of energy available for MHD energy generation decreased when the number of passes through the atmosphere increased, despite an increase in the time in atmosphere. This drop in energy can be most directly attributed to the strong dependence of electron number density on velocity and altitude. For the higher pass cases, comparatively more time is spent at lower velocities, resulting in lower overall electron number densities and thus available energy.

However, although the higher pass cases result in lower available energy, the rate at which that energy is generated is much more amenable to conventional energy storage systems. For example, for the Mars Science Laboratory case, there is a significant difference in the minimum power and energy density required to store the energy in under 10% of initial vehicle mass, a factor of about 4 for power density and 1.5 for energy density as opposed to a factor of roughly 1.5 for available energy. From an energy perspective, this result is unsurprising due to what is essentially the same velocity change occurring over a longer period of time.

In addition, the highest available energy per m<sup>2</sup> of generator area corresponded to the Moses test vehicle, which was also the vehicle configuration with the highest ballistic coefficient. The ballistic coefficient determines the rate at which the velocity decreases, and higher ballistic coefficients allow the vehicle to stay at higher velocities for longer during a multi-pass trajectory, resulting higher electron number densities and higher available power. The lowest ballistic coefficient vehicle, the Mars Science Laboratory, also had the lowest available energy, but it should be noted that this was also the vehicle with the most surface area available for MHD energy generation.

The ten pass cases seemed most amenable to current energy storage technologies, with the smallest power and energy density required to stay under 10% of initial vehicle mass. The existing or soon to exist energy storage technology masses for each of these cases, assuming average performance for each energy storage type, are presented below as Table 8.

**Table 8 Energy Storage System Masses for 10 Pass Trajectory**

<b>EES Technology</b>	<b>Moses Test Vehicle</b>		<b>Mars Pathfinder</b>		<b>Mars Science Lab</b>	
	<b>Mass (kg)</b>	<b>Calculation Method</b>	<b>Mass (kg)</b>	<b>Calculation Method</b>	<b>Mass (kg)</b>	<b>Calculation Method</b>
<b>Li-Ion</b>	<b>866</b>	<b>Peak Power</b>	<b>671</b>	<b>Peak Power</b>	<b>629</b>	<b>Peak Power</b>
<b>Lead Acid</b>	<b>1291</b>	<b>Max Energy</b>	<b>861</b>	<b>Max Energy</b>	<b>802</b>	<b>Max Energy</b>
<b>NiCad</b>	<b>895</b>	<b>Peak Power</b>	<b>694</b>	<b>Peak Power</b>	<b>650</b>	<b>Peak Power</b>
<b>Capacitor</b>	<b>20448</b>	<b>Max Energy</b>	<b>13644</b>	<b>Max Energy</b>	<b>12706</b>	<b>Max Energy</b>
<b>Ultracapacitor</b>	<b>5901</b>	<b>Max Energy</b>	<b>3937</b>	<b>Max Energy</b>	<b>3667</b>	<b>Max Energy</b>
<b>SMES</b>	<b>18775</b>	<b>Max Energy</b>	<b>12528</b>	<b>Max Energy</b>	<b>11667</b>	<b>Max Energy</b>
<b>SMES w/ CNT</b>	<b>94</b>	<b>Max Energy</b>	<b>63</b>	<b>Max Energy</b>	<b>58</b>	<b>Max Energy</b>
<b>Flywheel</b>	<b>2582</b>	<b>Max Energy</b>	<b>1723</b>	<b>Max Energy</b>	<b>1604</b>	<b>Max Energy</b>

Indeed, some of the energy storage systems examined have masses that are far in excess of the initial vehicle mass, rendering them immediately infeasible for this application. Of all the energy storage system technologies examined, only superconducting magnetic energy storage with carbon nanotubes satisfies the less than 10% of initial vehicle mass constraint, highlighting the importance of energy storage system development for MHD energy generation during planetary entry.

## V. Conclusion

An analysis capability for MHD generator equipped entry descent and landing systems has been developed. This capability includes a trajectory model, Martian atmospheric model, and post shock chemical equilibrium code implementation. In addition, several configurations were examined to study the trade between configurations, multi-pass orbits, and energy storage system technologies. It was generally found that increased ballistic coefficients resulted in higher available energy per meter squared of generator energy and that multi-pass orbits tended to reduce the power requirements dramatically while having a moderate decrease in total available energy. Increased electrical energy storage system performance has been deemed critical to the success of the system, with all but the most advanced prospective energy storage systems failing to be under 10% of initial vehicle mass. Future plans include extension of the model with a finite rate chemistry model and magnetohydrodynamic flow code as well as examination of other, larger potential Mars entry vehicles.

## Acknowledgments

This work is funded through a NASA Space Technology Research Fellowship, grant number NNX13AL82H. In addition, the authors would like to thank Dr. Bradley Steinfeldt of the Space Systems Design Lab at the Georgia Institute of Technology and Dr. Robert Moses of NASA Langley research center for their advice towards the completion of this work.

## References

- <sup>1</sup>Braun, R.D., Manning, R.M., *Mars Exploration Entry, Descent and Landing Challenges*, IEEE Aerospace Conference, 4-11 March 2006.
- <sup>2</sup>Spencer, D., Blanchard, R., Braun, R., *Pathfinder Entry, Descent, and Landing Reconstruction*, AIAA Journal of Rockets, Vol. 36, No. 3, May-June 1999.
- <sup>3</sup>Jarvinen, P.O., *On the Use of Magnetohydrodynamics During High Speed Re-Entry*, AIAA Journal of Rockets, Avco-Everett Research Laboratory, Research Note 463, July 1964.
- <sup>4</sup>Moses, R.W., Kuhl, CA., and Templeton, J.D., *Plasma Assisted ISRU at Mars*, 15th International conference on MHD Energy Conversion, Moscow, Russia, 24-27 May 2005.
- <sup>5</sup>Macheret, S.O., Shneider, M.N., Candler, G.V., Moses, R.W., and Kline, J.F., *Magnetohydrodynamic Power Generation for Planetary Entry Vehicles*, 35th AIAA Plasmadynamics and Lasers Conference, Portland, Oregon, 28 June – 1 July 2004.
- <sup>6</sup>Vuskovic, L., Popovic, S., Drake, J., and Moses, R.W., *Magnetohydrodynamic Power Generation in the Laboratory Simulated Martian Entry Plasma*, 15th International conference on MHD Energy Conversion, Moscow, Russia, 24-27 May 2005.
- <sup>7</sup>Popovic, S., Moses, R.W., and Vuskovic, L., *System Development for Mars Entry In Situ Resource Utilization*, 8th Interplanetary Probe Workshop, Portsmouth, VA, 6-10 June 2011.
- <sup>8</sup>Sparacino, et. al, *Survey of Battery Energy Storage Systems and Modeling Techniques*, IEEE Power and Energy Society General Meeting, San Diego, California, 22-26 July 2012.
- <sup>9</sup>Repic, E.M., Boobar, M.G., and Chapel F.G., *Aerobraking as a Potential Planetary Capture Mode*, AIAA Journal of Spacecraft, Vol. 5, No. 8, August 1968.
- <sup>10</sup>Johnston, et. al, *Mars Global Surveyor Aerobraking at Mars*, AAS/AIAA Space Flight Mechanics Meeting, Monterey, California, 9-11 February 1998.
- <sup>11</sup>Smith, J. C. and Bell, J. L., *2001 Mars Odyssey Aerobraking*, AIAA Journal of Spacecraft and Rockets, Vol. 42, No 3, May-June 2005.
- <sup>12</sup>Lyons, D. T., *Mars Reconnaissance Orbiter: Aerobraking Trajectory*, AIAA/AAS Astrodynamics Specialist Conference and Exhibit, Monterey, California, 5-8 August 2002.
- <sup>13</sup>S. Gordon and B. J. McBride, "Computer Program for Calculation of Complex Chemical Equilibrium Compositions and Applications," NASA Reference Publication 1311, 1996.
- <sup>14</sup>Mahaffy et al., "Abundance and Isotopic Composition of Gases in the Martian Atmosphere from the Curiosity Rover," Science, Vol. 341, No. 6143, page 263-266, July 2013.
- <sup>15</sup>Candler, G., "Computation of Thermo-Chemical Nonequilibrium Martian Atmospheric Entry Flows," AIAA/ASME 5<sup>th</sup> Joint Thermophysics and Heat Transfer Conference, Seattle, WA, June 18-20, 1990.
- <sup>16</sup>Chen, H., et. al, *Progress in Electrical Energy Storage System: A Critical Review*, Progress in Natural Science, Vol. 19, Issue 3, pages 291 - 312, 10 March 2009.
- <sup>17</sup>LyTec, LLC, *Flight-Weight Magnets Using Carbon Nanotubes*, LyTec-R-02-012, 2 May 2002.
- <sup>18</sup>Ribeiro, et. al., *Energy Storage Systems for Advanced Power Applications*, IEEE, Vol. 89, No. 12, page 1745, December 2001.